Study of an Asymmetric Flap Nozzle as a Thrust-Vectoring Device

C. C. Wu*
California State University, Los Angeles, California
and
W. L. Chow†
University of Illinois, Urbana-Champaign, Illinois

The problem of isentropic flow through an asymmetric two-dimensional convergent nozzle as a thrust-vectoring device has been solved by the method of hodograph transformation coupled with finite-difference computation. With the given appropriate flow parameters, the solution was first established in the hodograph domain. The corresponding nozzle configuration and the flowfield properties were subsequently obtained through direct integration. The thrust-vectoring performance corresponding to specific nozzle geometries were also determined and presented. Experiments for specific nozzle configurations were also conducted to obtain pressure data along the nozzle walls for verification purposes. The numerical results were found to be in good agreement with the experimental data.

Nomenclature

C_p = pressure coefficient
C_T = thrust coefficient
h_A = thickness of approaching uniform flow
h_E = thickness of asymtoptic uniform flow
M = Mach number
M^* = Mach number based on critical sound speed
p = pressure
q = transformed velocity
s = distance along nozzle wall
T = thrust force
V = velocity magnitude
x,y = physical coordinates
α_U,α_L = upper and lower flap angles
β = dimensionless flow angle
γ = specific heat ratio
δ = thrust angle
θ = flow angle
ρ = density
ϕ = potential function
ψ = stream function
ω = dimensionless velocity

Subscripts

A = approaching uniform flow
E = asymtoptic uniform flow (for subcritical flow)
E = critical point on sonic line (for supercritical flow)
0 = stagnation condition
∞ = freestream condition

Introduction

As the need for generating vectored thrust for modern V/STOL aircraft arises, propulsive nozzles of asymmetric geometries appear to be attractive. Also, as a result of more favorable interference with the slipstream, nozzles of two-dimensional configurations are being seriously considered. In recent years, various designs of asymmetric nozzles have been tested.[1-8] These investigations show that two-dimensional asymmetric nozzles have favorable aerodynamic effects on the aircraft in addition to their thrust-vectoring capability. They possess definite advantages over conventional axisymmetric nozzles in terms of aircraft maneuverability, airframe/nozzle integration, and potential for innovations and further development.

Being simple in design and inexpensive to fabricate, the flap nozzle (Fig. 1) is certainly a potential thrust-vectoring device. With the adjustable flap angles and relative positions, it is able to generate a wide variety of asymmetric flow patterns. This paper proposes a numerical treatment to solve the flowfield and to determine its thrust-vectoring performance as a function of the angles, lengths, and relative positions of the flaps. It is to be noted that, since no approximations are involved, the method of solution is exact (other than possible numerical errors).

Hodograph Transformation

In spite of the simplicity in design, it is difficult to obtain a direct solution of the flowfield due to the nonlinearity of the gasdynamic equation, the existence of a transonic flow region at the nozzle exit, and the unknown free jet boundaries. Nevertheless, in recent years, studies by Chow et al.[9-11] indicate that the method of hodograph transformation is particularly efficient for two-dimensional inviscid flow problems, especially when straight boundaries are involved.

For steady, irrotational flow of a perfect gas through the flap nozzle, the solution can be established by solving the

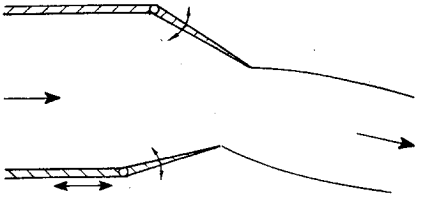

Fig. 1 Two-dimensional flap nozzle.

Presented as Paper 84-1360 at the AIAA/SAE/ASME 20th Joint Propulsion Conference, Cincinnati, Ohio, June 11-13, 1984; received Aug. 10, 1984; revision received March 25, 1985.

*Assistant Professor of Mechanical Engineering (formerly Graduate Assistant, University of Illinois, Urbana, Ill.). Member AIAA.

†Professor of Mechanical Engineering. Associate Fellow AIAA.

linear hodograph equation,[12]

$$V^2\psi_{VV}+V(1+M^2)\psi_V+(1-M^2)\psi_{\theta\theta}=0 \tag{1}$$

where the subscripts denote partial differentiations. The solution in the physical plane can then be obtained by integrating the following equations of transformation:

$$dx=\left(\frac{\cos\theta}{V}\phi_V-\frac{\rho_0}{\rho}\frac{\sin\theta}{V}\psi_V\right)dV+\left(\frac{\cos\theta}{V}\phi_\theta-\frac{\rho_0}{\rho}\frac{\sin\theta}{V}\psi_\theta\right)d\theta \tag{2a}$$

$$dy=\left(\frac{\sin\theta}{V}\phi_V-\frac{\rho_0}{\rho}\frac{\cos\theta}{V}\psi_V\right)dV+\left(\frac{\sin\theta}{V}\phi_\theta-\frac{\rho_0}{\rho}\frac{\cos\theta}{V}\psi_\theta\right)d\theta \tag{2b}$$

where

$$\phi_V=-\frac{\rho_0}{\rho}\frac{(1-M^2)}{V}\psi_\theta,\quad \phi_\theta=\frac{\rho_0}{\rho}V\psi_V \tag{3}$$

Since the features of subsonic and supersonic discharge are entirely different, the treatments for subcritical and supercritical flows are described separately below.

Subcritical Flow

For back pressure ratios higher than the critical value,

$$\frac{p^*}{p_0}=\left(\frac{2}{\gamma+1}\right)^{\gamma/(\gamma-1)}$$

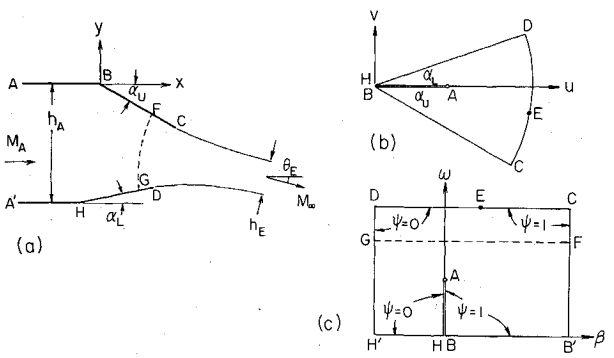

Fig. 2 Subcritical flow: a) physical plane, b) hodograph, c) computational plane.

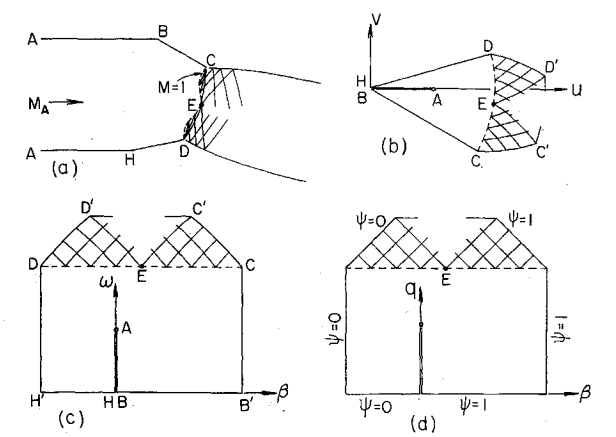

Fig. 3 Supercritical flow (unchoked): a) physical plane, b) hodograph, c) $\beta-\omega$ plane, d) computational plane.

the entire flowfield is subsonic and a uniform jet is found far downstream, as shown in Fig. 2a. The corresponding hodograph is shown in Fig. 2b. Upon introducing the dimensionless variables

$$\beta=\theta/\alpha_U,\quad \omega=V/V_\infty \tag{4}$$

the hodograph becomes a rectangle (Fig. 2c) and the hodograph equation assumes the form

$$\omega^2\psi_{\omega\omega}+\omega(1+M^2)\psi_\omega+(1-M^2)\psi_{\beta\beta}/\alpha_U^2=0 \tag{5}$$

The boundary conditions for Eq. (5) are also clearly specified in Fig. 2c. The Mach number can be directly expressed in terms of the independent variable ω through

$$M^2=\frac{2M^{*2}/(\gamma+1)}{1-M^{*2}/G} \tag{6}$$

where

$$G=\frac{(\gamma+1)}{(\gamma-1)},\quad M^{*2}=\frac{\omega^2(\gamma+1)M_\infty^2}{2+(\gamma-1)M_\infty^2}$$

The transformation from the (β,ω) plane to the (x,y) plane is now given by

$$dx=-(f_1\psi_\beta+f_2\psi_\omega)d\omega+(f_3\psi_\omega-f_2\psi_\beta)d\beta \tag{7a}$$

$$dy=-(g_1\psi_\beta-g_2\psi_\omega)d\omega+(g_3\psi_\omega+g_2\psi_\beta)d\beta \tag{7b}$$

where x and y are already normalized by h_A and

$$f_1(\beta,\omega)=\frac{\rho_0}{\rho}\frac{\cos(\alpha_U\beta)}{\alpha_U\omega^2}(1-M^2)$$

$$g_1(\beta,\omega)=\frac{\rho_0}{\rho}\frac{\sin(\alpha_U\beta)}{\alpha_U\omega^2}(1-M^2)$$

$$f_2(\beta,\omega)=\frac{\rho_0}{\rho}\frac{\sin(\alpha_U\beta)}{\omega}$$

$$g_2(\beta,\omega)=\frac{\rho_0}{\rho}\frac{\cos(\alpha_U\beta)}{\omega}$$

$$f_3(\beta,\omega)=\frac{\rho_0}{\rho}\alpha_U\cos(\alpha_U\beta)$$

$$g_3(\beta,\omega)=\frac{\rho_0}{\rho}\alpha_U\sin(\alpha_U\beta)$$

Supercritical Flow

For back pressures slightly lower than the critical pressure, the free jet is supersonic and a sonic line exists at the nozzle exit, as shown in Fig. 3a. The curved sonic line is to be interfered with the expansion fans generated from the nozzle lips and the waves reflected from the jet boundaries. Since the pattern of this wave system varies as the back pressure is changed, the sonic line is by no means frozen and the nozzle is still unchoked. Figure 3b shows the corresponding hodograph for an unchoked supercritical flow.

However, if the back pressure is sufficiently low, none of the reflected waves from the jet boundaries are able to intersect with the sonic line, as illustrated in Figs. 4a and 4b. Further reduction of the back pressure would have no effect on the sonic line; thus, the nozzle is choked.

It is clear from Fig. 4b that the velocities at points C′ and D′ depend upon the position of the critical point E, which is the only point on the sonic line where waves of opposite

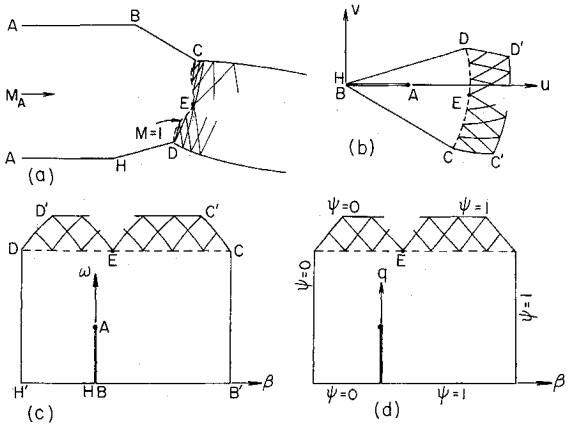

Fig. 4 Choked flow: a) physical plane, b) hodograph, c) $\beta-\omega$ plane, d) computational plane.

families generated from the two nozzle lips meet. Due to possible varieties of asymmetric configurations, this point may fall anywhere on the sonic line between the nozzle lips (C and D). For a specified set of flap angles and flow angle at E, the variation of Mach number along each wave can be determined from the well-known simple wave relation,[12]

$$\theta=-\sqrt{G}\tan^{-1}\sqrt{(M^2-1)/G}+\tan^{-1}\sqrt{(M^2-1)}+\text{const} \quad (8)$$

The chocked pressure ratio, which corresponds to the Mach number at C′ or D′(whichever is further from E), is readily given by the isentropic relation. Figure 5 summarizes the dependence of the chocked pressure ratio on the parameters $\theta_E'(=\theta_E+\alpha_U)$ and $\alpha_{UL}(=\alpha_L+|\alpha_U|)$.

For supercritical flows, it is most convenient to choose the sonic velocity as the reference velocity. Thus, the following dimensionless variables are introduced:

$$\beta=\theta/\alpha_U, \quad \omega=V/V^*=M^* \quad (9)$$

Equations (1) and (2) are thus reduced into dimensionless forms precisely the same as Eqs. (5) and (7), except that the Mach number is directly related to ω by the isentropic relation

$$M^2=\frac{2\omega^2/(\gamma+1)}{1-\omega^2/G}$$

As shown in Figs. 3c and 4c, the subsonic flow region upstream of the sonic line now becomes a rectangle, whereas the downstream supersonic region is governed by the method of characteristics. For the right-running waves,

$$\beta=f(\omega)+\text{const} \quad (10a)$$

and for the left-running waves,

$$\beta=-f(\omega)+\text{const} \quad (10b)$$

where

$$f(\omega)=-\frac{1}{\alpha_U}\left(\sqrt{G}\tan^{-1}\sqrt{\frac{\omega^2-1}{G-\omega^2}}-\tan^{-1}\sqrt{\frac{\omega^2-1}{1-\omega^2/G}}\right)$$

For convenience of finite difference computation, it is more desirable to transform this network of curved hodograph characteristics into straight lines through the transformation

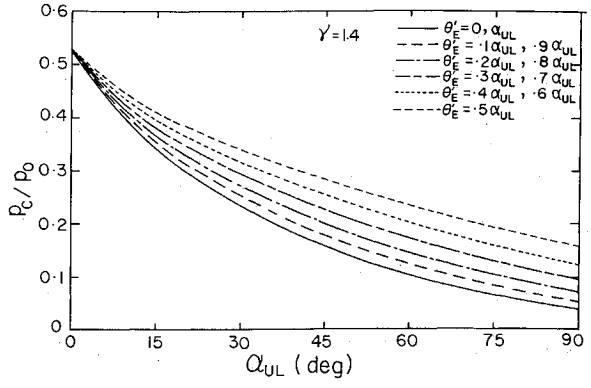

Fig. 5 Variation of choked pressure ratio.

of

$$q=\omega \quad \text{for} \quad \omega\le 1 \quad (11a)$$

$$q=f(\omega) \quad \text{for} \quad \omega>1 \quad (11b)$$

The domain of concern in the (β,q) plane and the necessary boundary conditions are shown in Figs. 3d and 4d for unchoked and choked flows, respectively.

The final form of the hodograph equation in the (β,q) plane can now be derived. For the subsonic region ($\omega\le 1$), it remains in the same form as given by Eq. (5), namely,

$$q^2\psi_{qq}+q(1+M^2)\psi_q+\frac{1-M^2}{\alpha_U^2}\psi_{\beta\beta}=0 \quad (12a)$$

For the supersonic region ($\omega>1$), the governing equation becomes

$$\frac{1}{\alpha_U}(\omega^2-1)\psi_{qq}-\frac{2\omega^4}{(\gamma-1)\sqrt{G(\omega^2-1)(G-\omega^2)}}\psi_q+\frac{1-\omega^2}{\alpha_U^2}\psi_{\beta\beta}=0 \quad (12b)$$

Upon introducing Eq. (11b), transformation of the supersonic region from the (β,q) plane to the (x,y) plane is found to be given by

$$dx=-[f_1\psi_\beta+f_2f'(\omega)\psi_q]\frac{dq}{f'(\omega)}+[f_3f'(\omega)\psi_q-f_2\psi_\beta]d\beta \quad (13a)$$

$$dy=-[g_1\psi_\beta-g_2f'(\omega)\psi_q]\frac{dq}{f'(\omega)}+[g_3f'(\omega)\psi_q+g_2\psi_\beta]d\beta \quad (13b)$$

while transformation for the subsonic region remains in the same form as given by Eq. (7).

Numerical Computation

Subcritical Flow

For subcritical flow, the governing equation is elliptic throughout the flowfield. With a given nozzle geometry, approaching flow condition and back pressure ratio, the asymptotic flow angle θ_E is unknown. Since elliptic flow is of the boundary value character, the solution cannot be established before θ_E is specified. Thus, under the condition of a prescribed nozzle configuration, θ_E can be found only through

iterations. This is usually accomplished by selecting a value for θ_E and subsequently determining the physical flowfield as described later in this section. Satisfaction of the momentum principle for the entire flowfield will determine the correct value of θ_E through trial and error. This iteration can be a rapidly convergent process.

Inasmuch as the hodograph transformation is an indirect approach, it has been found to be more efficient to specify θ_E rather than the complete nozzle geometry. Results from computation will produce the corresponding flap lengths and their relative positions. In this way, the trial and error procedures are entirely eliminated.

Upon subdividing the rectangular hodograph domain (Fig. 2c) into a finite difference mesh of uniform size in both directions, the finite difference form of Eq. (5) can be established and subsequently rearranged into the following convenient form:

$$\psi_{i,j+1}(\omega_j^2+A_j)-2\psi_{i,j}(\omega_j^2+B_j)+\psi_{i,j-1}(\omega_j^2-A_j)$$
$$=-B_j(\psi_{i+1,j}+\psi_{i-1,j}) \tag{14}$$

where

$$A_j=\frac{\Delta\omega}{2}(1+M_j^2)\omega_j \quad \text{and} \quad B_j=\frac{\Delta\omega^2}{\alpha_U^2\Delta\beta^2}(1-M_j^2)$$

For a given set of γ, α_U, α_L, β_E, ω_A, and M_∞ values, the coefficients in the above equation and the boundary conditions are completely specified. The value of ψ at each grid point within the domain can be found by successive overrelaxation (SOR) scheme. Calculation may be terminated when the variation of ψ at each grid point is less than an arbitrarily small value, say 10^{-5}. Once the ψ field is established, its derivatives (ψ_β and ψ_ω) at all points can be evaluated by finite difference and the solution can subsequently be transformed back to the physical plane through integration of Eq. (7) as follows:

1) The reference length h_A is found by integrating the equations from B′ first along the constant β line to any intermediate point F above point A and subsequently along the constant ω line (as shown by the dotted line F-G in Fig 2c) until the boundary H′-D is reached. Finally, integration is performed along the constant β line to H′.

2) Upon integrating the equations along the boundaries B′-C and H′-D, the flap lengths are obtained. Along with the specified flap angles, the nozzle geometry is uniquely defined.

3) The physical profile of the free jet boundaries can be traced by integrating the equations along boundaries C-E and D-E.

4) Finally, integration performed along constant ω lines traces the variation of velocity throughout the flowfield.

Once the thickness of the asymptotic uniform flow is determined, the thrust coefficient can readily be found as

$$C_T=\frac{T}{\frac{1}{2}\rho_\infty V_\infty^2 h_A}=2\left(\frac{h_E}{h_A}\right) \tag{15}$$

Supercritical Flow

For a specified nozzle geometry, approaching flow condition, and back pressure ratio, the flow angle at the critical point E on the sonic line is still unknown. An iterative process must be formulated to determine the correct value of θ_E if the nozzle configuration is to be completely specified. Again, such an iteration can be a rapidly convergent process. However, it has been found to be more efficient to specify β_E (in addition to γ, α_U, α_L, and M_∞) instead of the nozzle lengths and their relative positions. Successful application of hodograph transformation would yield the corresponding nozzle geometry.

The subsonic region in the (β,q) plane is likewise subdivided into a uniform finite difference mesh and the two families of

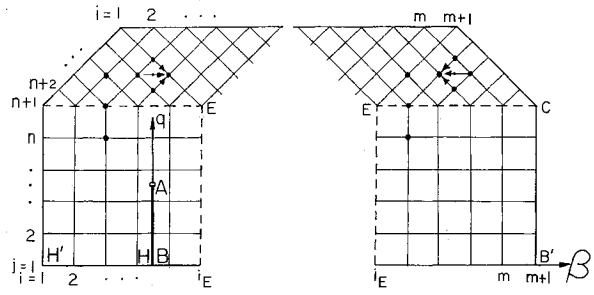

Fig. 6 Finite difference mesh for supercritical flow calculation.

characteristics are generated accordingly for the supersonic region, as illustrated in Fig. 6. For the grid points in the subsonic region ($\omega<1$), the finite difference scheme is identical to Eq. (14). For those points on the sonic line $\omega=1$, Eq. (12a) can be written into the finite difference form (referring to Fig. 6)

$$\Delta\omega(1+\Delta\omega)\psi_{i_1,n+3}-[\Delta\omega(1+\Delta\omega)+\Delta\omega_+(1-\Delta\omega_+)]\psi_{i,n+1}$$
$$+\Delta\omega_+(1-\Delta\omega_+)\psi_{i,n}=0 \tag{16}$$

with

$$\Delta\omega_+=\omega_{n+3}-\omega_{n+1}$$

where $i_1=i-1$ for $i<i_E$ and $i_1=i+1$ for $i>i_E$.

For the supersonic region $\omega>1$, the second-order finite difference form of Eq. (12b) written for the centroid of a typical cell (referring to Fig. 6) can be rearranged into the following algebraic relations. For the characteristics generated from the corner C toward E,

$$\psi_{i,j}=\psi_{i+1,j+1}+\psi_{i,j-1}-\psi_{i+1,j}-g(\omega_j)(\psi_{i+1,j+1}-\psi_{i,j-1}) \tag{17a}$$

and for the characteristics generated from corner D toward E,

$$\psi_{i,j}=\psi_{i-1,j+1}+\psi_{i,j-1}-\psi_{i-1,j}-g(\omega_j)(\psi_{i-1,j+1}-\psi_{i,j-1}) \tag{17b}$$

where

$$g(\omega)=\frac{\alpha_U\Delta\beta\omega^4}{2(\gamma-1)(\omega^2-1)\sqrt{G(\omega^2-1)(G-\omega^2)}}$$

Equations (17) essentially replace the characteristic relations. When the sequence of computations follows the directions as indicated in Fig. 6, quantities on the right side are known and $\psi_{i,j}$ can readily be computed.

For a given set of γ, α_U, α_L, ω_A, β_E, and M_∞ values, the boundary conditions and the coefficients in Eqs. (14), (16), and (17) are completely specified. The value of ψ at each internal grid point can now be determined by successive iterations for the subsonic region [governed by Eqs. (14) and (16)], coupled with repeated application of Eqs. (17) for the cells in the supersonic region. The physical profiles of the nozzle, free jet, constant Mach lines, and all other flow characteristics are subsequently obtained by integrating Eqs. (7). The integrating procedures are similar to those for subcritical computations.

Finally, the horizontal and vertical components of the thrust coefficient can be evaluated as

$$C_{T,H}=\frac{T_H}{\frac{1}{2}\rho^* V^{*2} h_A}=C_{p\infty}(y_D-y_C)+2\int_D^C \cos(\theta-\nu)\cos\theta\,dl$$

$$C_{T,V}=\frac{T_V}{\frac{1}{2}\rho^* V^{*2} h_A}=C_{p\infty}(x_D-x_C)-2\int_D^C \cos(\theta-\nu)\sin\theta\,dl$$

where

$$C_{p\infty}=\frac{2}{\gamma}\left(\frac{p_\infty}{p^*}-1\right),\quad \nu=-\tan^{-1}\frac{dx}{dy},\quad dl=\sqrt{dx^2+dy^2}$$

The thrust coefficient and the thrust angle can then be determined as

$$C_T=\frac{T}{\frac{1}{2}\rho^* V^{*2} h_A}=\sqrt{C_{T,H}^2+C_{T,V}^2}\ \text{and}\ \delta=\tan^{-1}(C_{T,V}/C_{T,H})$$

Typical Results

Nozzle Configuration and Flowfield

Results of a subcritical case and a supercritical case are shown in Figs. 7 and 8, respectively. A 40×20 finite difference mesh was employed for the subcritical calculation, while a 40×40 system was used for the supercritical calculation. For typical subcritical cases, about 3.5 s computation time is required to produce a complete set of results on the Cyber 175 computer. For supercritical cases, a computation time of 15-20 s (depending on the back pressure ratio) is needed.

It has been learned that over-relaxation significantly improves the convergent rate for subcritical calculations. With a relaxation factor of 1.6, about 100 iterations were required to obtain the converged ψ values. It has also been found that over-relaxation would delay or upset convergence for supercritical calculations. Typically, about 200-300 iterations were needed to stablize the ψ values for a supercritical case.

Thrust-Vectoring Performance

By varying one or more of the parameters α_U, α_L, ω_A, β_E, and M_∞, numerous nozzle geometries and the associated flowfields and vectored thrusts can be obtained. Figure 9 summarizes the resulting performance of a choked nozzle with equal flap lengths and a fixed upper flap angle. The variation of the thrust vector with the lower flap angle is shown.

Limiting Cases

Referring to Fig. 2c, the limiting cases for subcritical flows can be easily realized when point E coincides with point C or

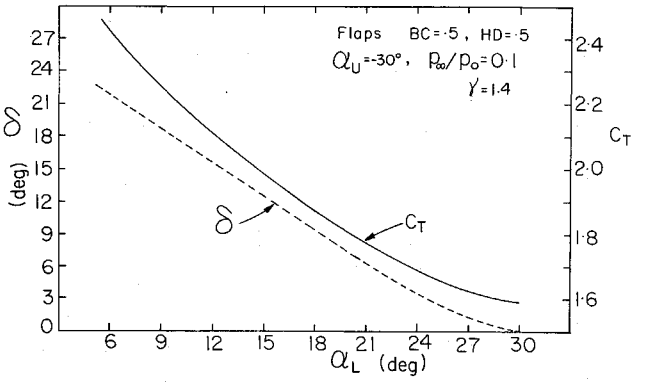

Fig. 9 Thrust-vectoring performance of a typical flap nozzle.

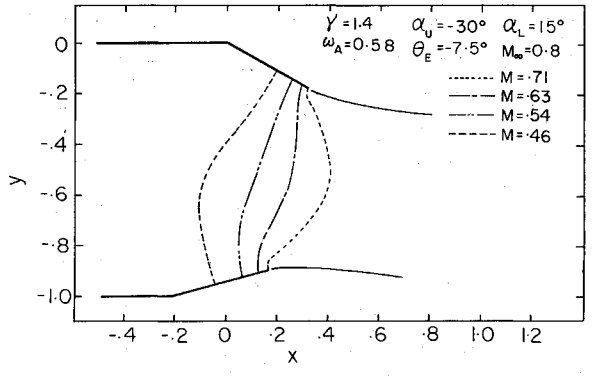

Fig. 7 Solution of a typical subcritical flow.

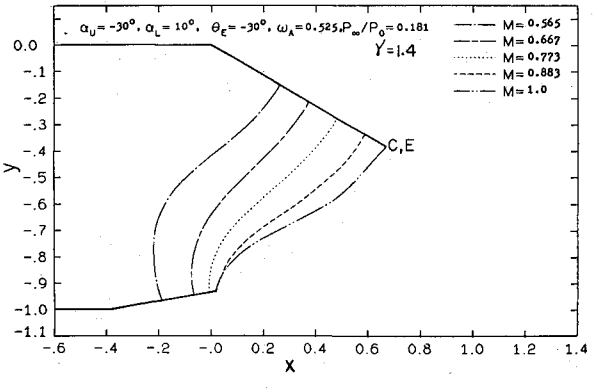

Fig. 10 Solution of a typical limiting case.

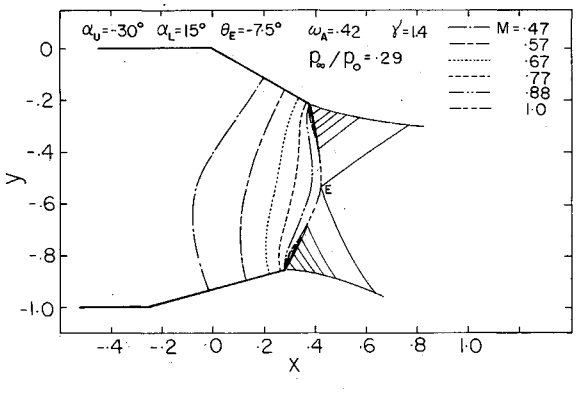

Fig. 8 Solution of a typical choked flow.

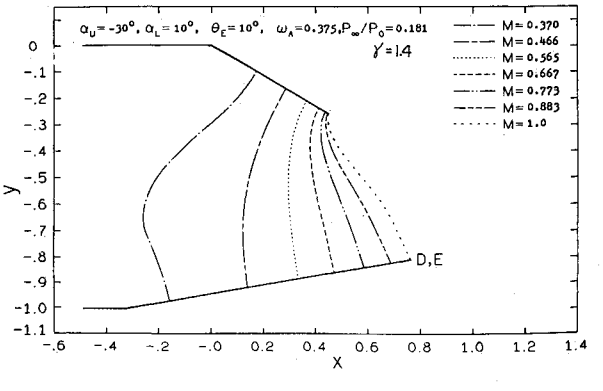

Fig. 11 Solution of a typical limiting case.

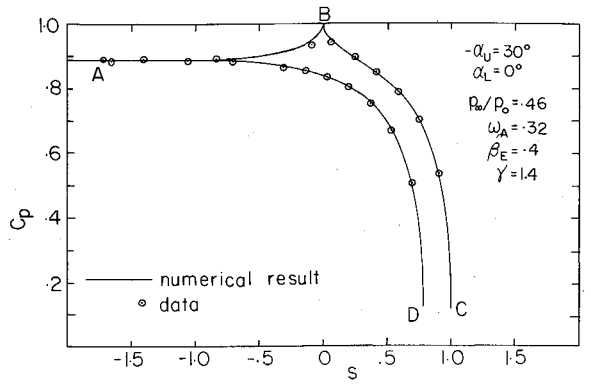

Fig. 12 Pressure distribution along nozzle walls.

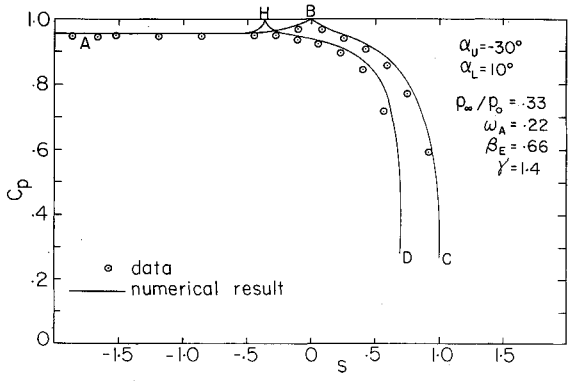

Fig. 13 Pressure distribution along nozzle walls.

D. Theoretically, these cases can be achieved only by an infinitely long upper or lower flap.

For supersonic flows, the limiting condition occurs when the critical point E coincides with one of the nozzle lips (C or D). One can infer from Figs. 10 and 11, where two typical limiting cases are shown, that the sonic line is interacting with waves of a single family. If the lower flap is moved further upstream (or downstream) beyond its limiting position as shown in Fig. 10 (or 11), the critical point will fall on the upper (or lower) flap. In the extreme, the sonic line may even appear upstream of one of the hinges (B and H) so that a curved shock will be generated. This is certainly an undesirable nozzle configuration.

Verification of Solutions

The momentum principle was employed as a means to verify the numerical solutions. It is found to be satisfied for all cases considered, indicating that the results are satisfactory. Typical errors from the momentum equation are on the order of 10^{-3}.

Experiments for certain nozzle configurations were also conducted in the laboratories at the University of Illinois at Urbana-Champaign. Pressure data were taken along the nozzle walls and were compared with the pressure distribution obtained from numerical computation. Except for a very small recirculating flow region near the corner, excellent agreement between the two was observed. Figures 12 and 13 show results of two typical supercritical tests.

Conclusion

Although it is an inverse method, hodograph transformation proved to be an effective tool for solving two-dimensional mixed-flow problems. Consistency with experimental results and relatively short computing time indicate that the numerical scheme developed is reliable and economical. The potential of this method when applied to other flow problems needs to be further explored. It is expected that, with some modification, it may be applied to study some of the nozzles proposed in Refs. 1-8, such as two-dimensional convergent-divergent, two-dimensional wedge, and ADEN nozzles.

This study also shows that the asymmetric flap nozzle has significant thrust-vectoring capability. With its simplicity of design and control, it certainly appears to be a promising thrust-vectoring device.

It is also interesting to note that when the jet/slipstream interaction is taken into account, it may result in different pressure levels impressed on opposite sides of the jet. Previous experience gained in the study of base pressures[13] should be adequate to deal with this type of challenging problems.

Acknowledgment

This study was partially supported by the U.S. Army Research Office through Research Grant DAAG 29-79-C0184 and subsequently DAAG 29-83-K0043.

References

[1]Capone, F. J., "Exploratory Investigation of Lift Induced on a Swept Wing by a Two-Dimensional Partial-Span Deflected Jet at Mach Numbers from 0.20 to 1.30," NASA TM X-2529, 1972.

[2]Capone, F. J., "The Effects of Vectoring a Partial-Span Rectangular Jet on Propulsion-Induced Aerodynamics Forces at Mach Numbers from 0.40 to 1.20," NASA TN D-8039, 1975.

[3]Capone, F. J., "Effects of Nozzle Location and Shape on Propulsion-Induced Aerodynamic Characteristics Due to Vectoring Twin Nozzles at Mach Numbers from 0.40 to 1.20," NASA TM X-3313, 1975.

[4]Capone, F. J., "Supercirculation Effects Induced by Vectoring a Partial-Span Rectangular Jet," *Journal of Aircraft*, Vol. 12, Aug. 1975, pp. 633-638.

[5]Maiden, D. L. and Petit, J. E., "Investigation of Two-Dimensional Wedge Exhaust Nozzles for Advanced Aircraft," *Journal of Aircraft*, Vol. 13, Oct. 1976, pp. 809-816.

[6]Willard, C. M., Capone, F. J., Konarski, M., and Stevens, H. L., "Static Performance of Vectoring/Reversing Nonaxisymmetric Nozzles," *Journal of Aircraft*, Vol. 16, Aug. 1979, 116-123.

[7]Hiley, P. E., Kitzmiller, D. and Willard, C. M., "Installed Performance of Vectoring/Reversing Nonaxisymmetric Nozzles," *Journal of Aircraft*, Vol. 16, Aug. 1979, pp. 532-538.

[8]Laughrey, J. A., Drape, D. J., and Hiley, P. E., "Performance Evaluation of an Air Vehicle Utilizing Nonaxisymmetric Nozzles," *Journal of Aircraft*, Vol. 18, Feb. 1981, pp. 89-95.

[9]Chow, W. L. and Liu, S. K., "Numerical Solution of the Compressible Hodograph Equation," *AIAA Journal*, Vol. 16, Feb. 1978, pp. 188-189.

[10]Chow, W. L., Han, T., and Wu, C., "Hydrodynamics Solution for Incompressible Flow as Influenced by Gravitation," *AIAA Journal*, Vol. 16, Oct. 1978, pp. 1097-1098.

[11]Chow, W. L. and Han, T., "Inviscid Solution for the Problem of Free Overfall," *Transactions of ASME, Journal of Applied Mechanics*, Vol. 46, No. 1, 1979, pp. 1-5.

[12]Shapiro, A. H., "The Hodograph Method for Mixed Subsonic-Supersonic Flow," *The Dynamics and Thermodynamics of Compressible Fluid Flow*, Vol. 2, Ronald Press Co., New York, 1953.

[13]Chow, W. L., "Base Pressure of a Projectile within the Transonic Flight Regime," AIAA Paper 84-0230, 1984 (to be published in *AIAA Journal*).